PRELIMINARY RESULTS OF THE BEAM CONTROL AND DETECTION OF THE KIRAMS ELECTRON MICROBEAM SYSTEM

G.M. SUN, E.H. KIM* and K.B. SONG
Korea Institute of Radiological and Medical Sciences
Gongneung-dong, Nowon-gu, Seoul 139-706

J.W. JEONG and H.D. CHOI
Department of Nuclear Engineering, Seoul National University
Shillim-dong, Gwanak-gu, Seoul 151-742
*To whom correspondence should be addressed. ekim@kcch.re.kr

Received August 16, 2004
Accepted for Publication November 8, 2004

The Korea Institute of Radiological and Medical Sciences (KIRAMS) electron microbeam system has been built with its prototype components. The system is composed of an electron gun, a beam transport chamber, and a cell image acquisition and positioning stage. Each component has been upgraded through repetitive performance tests for various parametric arrangements. This paper presents the preliminary results of the performance test on the beam control and detection parts of the system.

KEYWORDS : electron microbeam system, individual cell targeting, low dose effect

1. INTRODUCTION

The use of microbeam techniques in radiobiology dates back to the 1920's with the work of Tschachotin who irradiated the spawn of sea urchins and frogs with X-ray and ultraviolet light. In 1953, Zirkle and Bloom designed and constructed a microbeam facility [1] that utilized a 2 MeV proton beam of 2.5 μm in diameter. Their facility, however, did not allow counting the radiation particles that entered individual target cells. Since then, various facilities utilizing protons, alpha particles, and heavy ions have been developed and improved through the technical advancements of optical lenses, particle delivery systems, beam focusing and detection systems, cell imaging systems, and computer controls. New techniques of assaying individual cellular response have further enhanced the biological research work performed in microbeam facilities.

The microbeam irradiation device for single cell targeting was devised originally to remove the statistical uncertainty regarding individual cells being hit by radiation in a low-dose environment [2]. The microbeam facilities developed in 1990's [3-5] have been used to study the cellular response to single cell targeting with protons, alpha particles, and X-rays. To date, the bystander effect [6] and genomic instability [7] have been the major observations of microbeam experiments. Utilizing an electron beam for microbeam experiments has been of interest in recent years [8-11], though any significant results have not been reported so far.

The Korea Institute of Radiological and Medical Sciences (KIRAMS) electron microbeam system is designed to enable the target cells in vitro to be selectively irradiated with low-energy, low-current electrons [9]. Though the basic scheme of the KIRAMS electron microbeam system is similar to that of other charged-particle microbeam systems, it must overcome additional difficulties, such as controlling an electron path under the influence of the environmental magnetic field, delivering low-energy electrons to the target cells through a scattering medium, and maintaining a stable, low-current electron beam. This paper describes the prototype components of the KIRAMS electron microbeam system and presents the preliminary results of the performance test on the beam control and detection.

2. SYSTEM COMPONENTS

Fig. 1 presents the present structure of the KIRAMS electron microbeam system. The system comprises (1) an

electron gun, (2) a beam transport chamber, and (3) a cell image acquisition and positioning stage. The components of the system are illustrated in detail in Fig. 2. The design requirements of an electron microbeam system to be used for studying low-dose radiation effects have been described in previous publications [9, 10].

Fig. 1. The KIRAMS Electron Microbeam System.

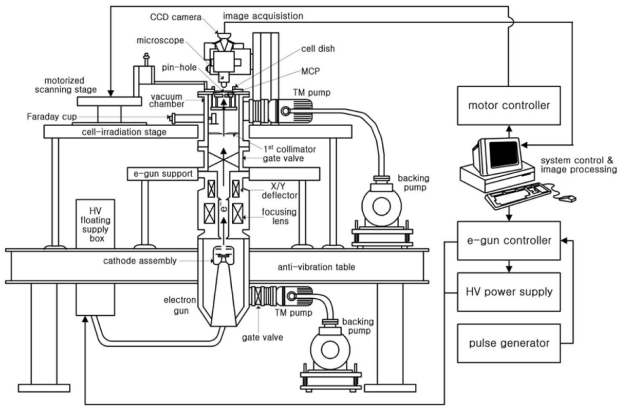

Fig. 2. Schematic Diagram of the Electron Microbeam cell-irradiation System.

The system employs a pulse electron beam for discrete beam emission. A Faraday cup is installed to monitor the source beam current at the front of the beam transport chamber. The beam is collimated to 2 mm in diameter. The final beam size is defined by the 5μm-diameter pin-hole at the exit of the beam transport chamber. There is a space reserved for a micro-channel plate (MCP) at the end of the beam transport chamber. The MCP is to be mounted for real-time monitoring of the electron beam during target cell irradiation. Two turbo molecular pumps are connected to the electron gun and to the beam transport chamber, respectively. The base pressures are 3.0×10^{-7} torr in the electron gun and 2.4×10^{-6} torr in the beam transport chamber.

The computer-controlled unit for cell image acquisition and positioning is composed of a Carl Zeiss Axiotech100 microscope, a CCD camera, and an image grabber. The IMAQ Vision 7.0 is used for cell image processing. The cells are cultured in a Mylar-bottom dish, which is specially designed to minimize the degradation of the low-energy electron beam. After the cell dish is placed in the dish holder, the CCD camera captures the image of the cells attached to the dish bottom. The relative positions of the cells to the beam exit are registered by pre-processing of the cell image data. The target cells, assigned by the operator, are moved individually to the beam exit. For micro-precision target cell positioning, an XY stage (65 $\times$50 mm) and an MCU-28 motor controller are mounted on the cell irradiation stage. The LabView 7.1 is employed to operate the MCU-28 motor controller and to control the electron source beam generation.

3. BEAM CONTROL

The performance of the electron gun in source beam extraction is investigated by varying its operation parameters. The source current of the cathode determines the emission current, which is induced by the electron emissions off the cathode. The emission beam enters the transport chamber to be collimated into a size appropriate for final use. We measured the beam current with the Faraday cup installed in the beam transport chamber. During the beam current measurement, the first anode voltage, the focusing lens current, and the X/Y deflector current are set for

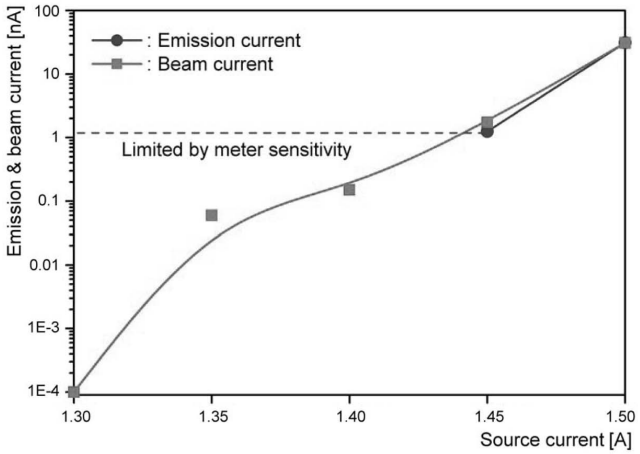

Fig. 3. Variation of the Emission Current and the Beam Current According to the Source Current for a 70 keV Electron Beam (lens current = 1.30 A, grid voltage = 50V, anode voltage = 900V).

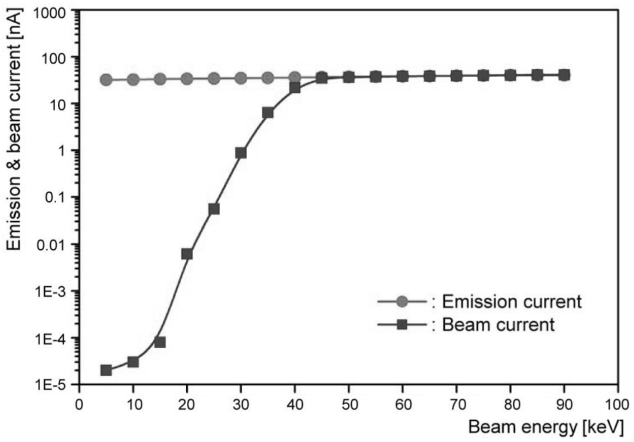

Fig. 4. Effect of the Beam Energy on the Emission Current and the Beam Current with Anode and Lens Set for Optimum Beam (source current = 1.50 A, grid voltage = 60V).

optimum beam collection at the Faraday cup.

Shown in Fig. 3 is the variation of emission current and beam current according to the source current for a 70 keV electron beam generation. The emission current reading was limited by a meter sensitivity of less than 1 nA. Fig. 4 shows how the emission current and the beam current vary with the electron beam energy. When the source current is held constant, the emission current varies little with the change in beam energy. Regarding the beam current, however, beam loss is observed at an electron energy of less than 45 keV. The loss of beam current is presumed to be caused by the collision of electrons with the high voltage shield and other structures.

The electron beam can easily deviate from its initial direction in a magnetic field. We investigated the field distribution in the laboratory and identified several sources of magnetic field in the peripherals. The primary magnetic sources included the electron beam device, the cold cathode gauge, and the turbo-molecular pump. By replacing the magnetic parts with non-magnetic parts and by taking shielding measures, we could limit the magnetic field in the beam transport chamber to about 200 mG, which is below the average earth magnetic field. The prototype beam-transport chamber was made of stainless steel, non-magnetic material, which permits magnetic field penetration into the vacuum. We estimated the influence of the magnetic field on the path of electron beam with a simple formula. Fig. 5 illustrates the possible deviation of an electron beam from its initial direction at emission from the electron gun. 70 keV electrons are expected to deviate from their initial direction by 2 mm after traveling a 45 cm-distance in vacuum. This deviation of 2 mm was satisfactorily compensated by the X/Y deflector. A fluorescent foil was placed at the end of the beam transport chamber to determine the beam alignment setting.

When the lens current is zero, the electron beam passes through the lens coil without any alteration in its path, making the focal plane infinite. As the lens current is increased, the periphery of the focal plane is changed. With the proper gun alignment, the focal plane varies in diameter but remains in its concentric circular form. When the beam alignment is inappropriate, the beam axis and the lens axis are not collinear and, consequently, the magnetic lens causes the rotation of the focal plane with a shift of its center. In addition, the focal plane may appear elliptical. The electron gun was tuned with the alignment screws on the electron gun chamber. The beam intensity profile defined by the pin-hole is shown in Fig. 6. The profile was obtained by placing a fluorescent foil on the exit of the pin-hole. The intensities of visible lights emitted from the fluorescent foil by

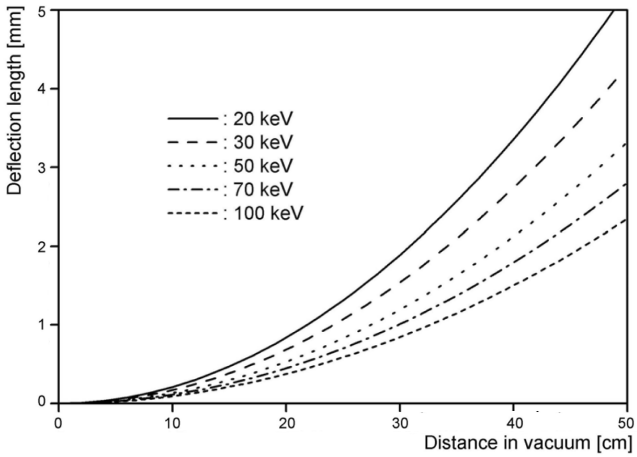

Fig. 5. Variation of the Deflection Length According to the Beam Transport Distance in Vacuum. B = 200 mG.

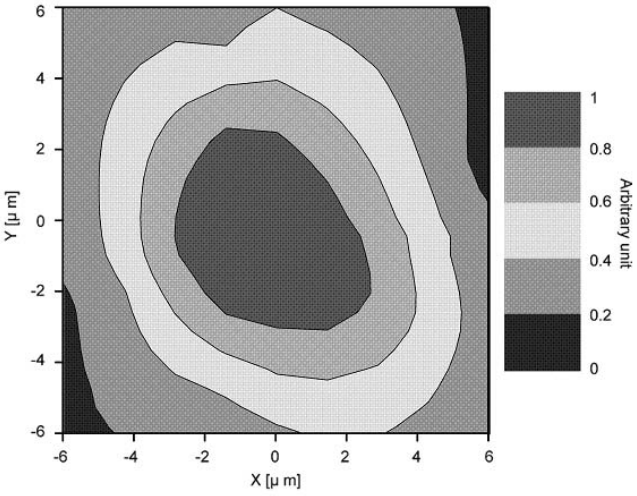

Fig. 6. Beam Intensity Profile at the Exit of the Pin-hole.

electron beam irradiation were registered by the CCD camera and normalized to the highest value. A new beam transport chamber is designed to be more compact and to be lined with a 2 mm-thick mu-metal sheet inside. The mu-metal, with high magnetic permeability, absorbs about 99 percent of the environmental magnetic field.

4. BEAM DETECTION

The KIRAMS electron microbeam system has been built to irradiate individual target cells with a selected number of electrons [9]. The number of electrons delivered to the target cell per single pulse beam is naturally in a statistical variation. The variation becomes more significant when a lower beam current is extracted. Since our goal is to investigate the cellular effects of low-dose radiation, the electron current delivered to the target cells needs to be kept as low as control will allow. As mentioned in a previous publication [10], the number of electrons to be delivered to individual target cells to simulate 0.2 Gy of cellular dose is some tens of electrons at 70 keV. A realistic description of target cell exposure to low-dose radiation necessitates an accurate count of the electrons incident on the individual target cells. It is desirable to detect the electrons entering the target cell in real time without degrading their characteristics.

Major facilities using protons or alpha particles can achieve real time detection, due to the high permeability of the particles at high energies. In the Columbia University's facility [3], for instance, high-energy protons and alpha particles produced by a 4-MV Van de Graaff accelerator can pass through a target cell with only small portion of their energy lost. Charged particles that escape the target cell are detected in real time, using a gas-filled ionization chamber mounted over the cell dish. In the Texas A&M's facility [12], on the other hand, the beam rates are determined in real time using an 8 μm-thick sheet of plastic scintillator placed between the aperture and the cell dish.

When dealing with low-energy electrons, real-time detection is not practical because most of the electron energy is lost within the target cell. In this study, we consider two methods of detecting the electrons incident on the target cell. The first method is to estimate the current of primary electrons entering the target cell by placing a PIPS detector at the exit of the vacuum window, over which the cell dish is to be positioned during the cell irradiation experiment. The second method is to take an indirect measurement of the primary electron current, by counting the secondary electrons emitted backward from the vacuum window material with an MCP.

Via measurement with a PIPS detector, we can obtain both the electron current data and the energy spectrum information. Presented in Fig. 7 are the electron spectra, one measured using the PIPS detector and the other obtained by an EGSnrc [13] simulation, for the 70 keV electron source beam. The ratio of the beam current to the peak count rate was maintained at about 1.2×10^3 cps/pA under optimized detection conditions. In both the measurement and the simulation, the full-energy electron peak is accompanied by a low-energy continuum. In the low energy continuum of the simulation data, the gray area is attributed to the backscattering and Bremsstrahlung occurring inside the PIPS, whereas the remaining area is thought to be caused by the electrons colliding with the structure around the pin-hole. From the simulation data, the full-energy electron peak was found to make up 76 % out of the total count. Bremsstrahlung and backscattering accounted for 16 %, whereas the remaining 8 % is attributed to the aperture scattering. Since the measured peak area coincides with the simulation peak area, we can determine the number of electrons incident on the PIPS detector by multiplying the measured peak count by the peak efficiency determined from the simulation data. The number of electrons incident on the PIPS detector, in turn, can be assumed to be the number of electrons delivered to the individual cells during the cell-irradiation experiment performed with the PIPS detector removed.

We also investigated the statistical characteristics of the full-energy electron peak count at the target cell position by using the PIPS detector and a multi-channel scaler (MCS). Fig. 8 shows the stability of the electron peak count when a pulse beam of 70 keV electrons is generated at a beam current of about 45 pA, with a repetition rate of 200 Hz and a beam width of 2 ms. It is observed in Fig. 9 that the statistical variation becomes

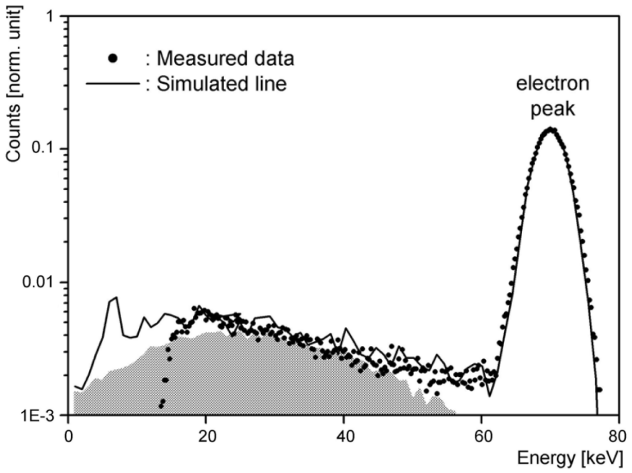

Fig. 7. The Electron Spectrum Measured Using the PIPS Detector Compared with that Obtained by Running the EGSnrc Code. In the Low-Energy Continuum of the Simulation Data, the Gray Area is Attributed to the Backscattering and Bremsstrahlung Occurring Inside the PIPS Whereas the Remaining area Counts for the Scattering by the Pin-Hole Structure.

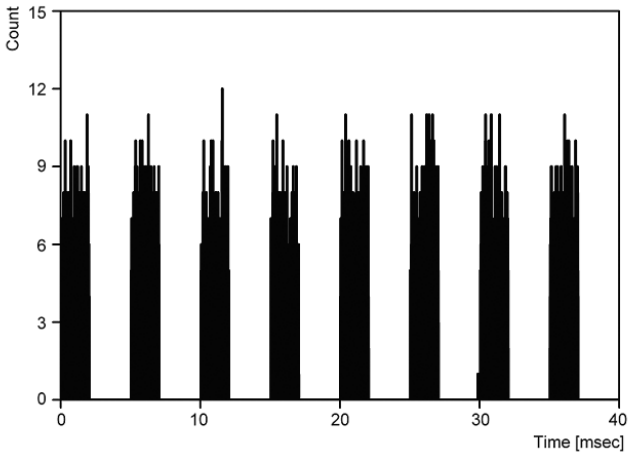

Fig. 8. Full Energy Electron Peak Counts in Pulse-mode Beam Operation (energy = 70 keV; emission current = 45 pA; beam width : 2 ms, repetition rate : 200 Hz).

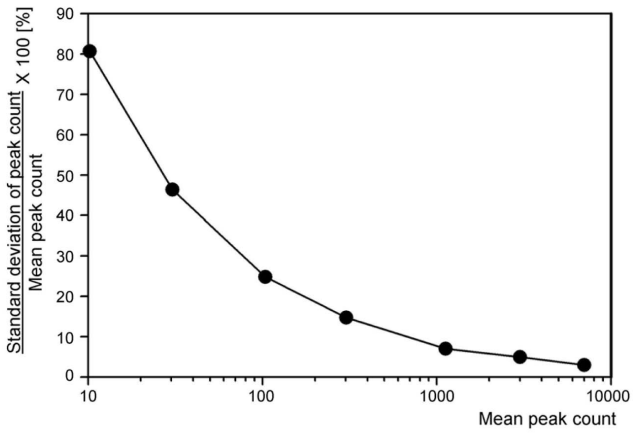

Fig. 9. The Standard Deviation of Peak Count According to the Mean Peak Count. Beam Energy is 70 keV.

more significant when the emission current or the mean number of electrons entering the target cell is decreased. When the mean peak count is 100, which corresponds to an absorbed dose of 0.2 Gy in the cell, the standard deviation is about 25%.

The current of secondary electrons measured with the MCP during the cell-irradiation experiment can be a useful probe for the real-time monitoring of primary electrons leaving the beam transport chamber toward the cell. However, it also has a drawback in that the surface condition of the vacuum window material changes and, thus, the yield of secondary electrons changes during the cell-irradiation. Our first experiment with the MCP was attempted recently. Characterization of the primary and the secondary electrons will be presented after further experiments.

5. CONCLUSION

The performance of beam control and beam detection for the KIRAMS electron-microbeam irradiation system was evaluated. The pulse-mode beam extraction and thus the control of the number of electrons entering into the target cells proved stable at each parametric arrangement during the electron gun operation. The PIPS detector provided reliable data when counting the electron beam current entering the target cells. Remaining problems include managing the statistical variation in the electron current entering the target cells under low-dose conditions and installing a real-time beam monitoring system. In addition, the system unit used for prompt cell image acquisition and precise cell positioning needs to be refined.

6. ACKNOWLEDGMENT

This work was financially supported by the Korea Ministry of Science and Technology (MOST) through its National Nuclear Technology Program.

REFERENCES

[1] R.E. Zirkle and W. Bloom. “Irradiation of parts of individual cells”, *Science*, **117**, 467 (1953).

[2] L.A. Braby and W.D. Reece, “Studying low dose effects using single particle microbeam irradiation”, *Radiat. Prot. Dosim.*, **31**, 311 (1990).

[3] G. Randers-Pehrson, C.R. Geard, G. Johnson, C.D. Elliston and D.J. Brenner. “The Columbia University single-ion microbeam”, *Radiat. Res.*, **156**, 210 (2001).

[4] M. Folkard, B. Vojnovic, K.M. Prise, A.G. Bowey, R.J. Locke, G. Schettino and B.D. Michael. “A charged-particle microbeam: I. Development of an experimental system for targeting cells individually with counted particles”, *Int. J. Radiat. Biol.*, **72**, 375 (1997).

[5] M. Folkard, G. Schettino, B. Vojnovic, S. Gilchrist, A.G. Michette, S.J. Pfauntsch, K.M. Prise and B.D. Michael. “A focused ultrasoft x-ray microbeam for targeting cells individually with submicrometer accuracy”, *Radiat. Res.*, **156**, 796 (2001).

[6] S.G. Sawant, G. Randers-Pehrson, C.R. Geard, D.J. Brenner and E.J. Hall. “The bystander effect in radiation oncogenesis: I. Transformation in C3H 10T1/2 cells in vitro can be initiated in the unirradiated neighbors of irradiated cells”, *Radiat. Res.*, **155**, 397 (2001).

[7] M.A. Kadhim, S.J. Marsden, D.T. Goodhead, A.M. Malcolmson, M. Folkard, K.M. Prise and B.D. Michael. “Long-term genomic instability in human lymphocytes induced by single-particle irradiation”, *Radiat. Res.*, **155**, 122 (2001).

[8] W.E. Wilson, D.J. Lynch, K. Wei, and L.A. Braby. “Microdosimetry of a 25 keV electron microbeam”, *Radiat. Res.*, **155**, 89 (2001).

[9] M.C. Choi, E.H. Kim, K.B. Song, D.H. Lee and S.W. Park, J.W. Jeong, G.M. Sun and H.D. Choi. “Design and operation specification of an electron microbeam system

for investing cellular radiation effect", *J. Nucl. Sci. and Tech.*, **Suppl**. **4**. 227 (2004).

[10] E.H. Kim, M. Chang, M.C. Choi and C.S. Kang. "Dosimetric aspects of the electron microbeam irradiation system for use in low-dose radiation effect study", *J. Nucl. Sci. and Tech.*, **Suppl**. **4**. 223 (2004).

[11] J.W. Jeong, G.M. Sun, H.D. Choi, E.H. Kim, M.C. Choi and H.B. Song. "Detection system in KIRAMS electron microbeam system", *Proc. Korean Nucl. Soc. Annual Meeting*, Yongpyong, Korea, Oct. 30-31, 2003.

[12] L.A. Braby, A.L. Brooks and N.F. Metting. "Cellular effects of individual high-linear energy transfer particles and implications for tissue response at low doses", *Radiat. Res.*, 148, S108 (1997).

[13] I. Kawrakow and D.W.O. Rogers. "The EGSnrc Code System: Monte Carlo Simulation of Electron and Photon Transport", Technical Report PIRS-701, National Research Council of Canada (2000).